FERMILAB-Pub-99/079-A

Large-Scale Power Spectrum and Cosmological Parameters from SFI Peculiar Velocities

Wolfram Freudling [1,2], Idit Zehavi [3,4],
Luiz N. da Costa [2,5], Avishai Dekel [3], Amiram Eldar [3], Riccardo Giovanelli [6],
Martha P. Haynes [6], John J. Salzer [7], Gary Wegner [8], and Saleem Zaroubi [3,9]

ABSTRACT

We estimate the power spectrum of *mass* density fluctuations from peculiar velocities of galaxies by applying an improved maximum-likelihood technique to the new all-sky SFI catalog. Parametric models are used for the power spectrum and the errors, and the free parameters are determined by assuming Gaussian velocity fields and errors and maximizing the probability of the data given the model. It has been applied to generalized CDM models with and without COBE normalization. The method has been carefully tested using artificial SFI catalogs. The most likely distance errors are found to be similar to the original error estimates in the SFI data. The general result that is not very sensitive to the prior model used is a relatively high amplitude of the power spectrum. For example, at $k = 0.1\,h\,\mathrm{Mpc}^{-1}$ we find $P(k)\Omega^{1.2} = (4.4 \pm 1.7) \times 10^3\ (h^{-1}\mathrm{Mpc})^3$. An integral over

[1]Space Telescope-European Coordinating Facility, European Southern Observatory, Karl-Schwarzschild Str. 2, D-85748 Garching b. München, Germany

[2]European Southern Observatory, Karl-Schwarzschild Str. 2, D-85748 Garching b. München, Germany

[3]Racah Institute of Physics, The Hebrew University, Jerusalem 91904, Israel

[4]NASA/Fermilab Astrophysics Group, Fermi National Accelerator Laboratory, Box 500, Batavia, IL 60510-0500

[5]Observatorio Nacional, Rua Gen. Jose Cristino 77, Rio de Janeiro, Brazil

[6]Center for Radiophysics and Space Research and National Astronomy and Ionosphere Center, Cornell University, Ithaca, NY 14953

[7]Dept. of Astronomy, Wesleyan University, Middletown, CT 06457

[8]Dept. of Physics and Astronomy, Dartmouth college, Hanover, NH 03755

[9]Max Planck-Institut für Astrophysik, Karl-Schwarzschild-Strasse 1, 65748 Garching, Germany.

the power spectrum yields $\sigma_8\Omega^{0.6} = 0.82 \pm 0.12$. Model-dependent constraints on the cosmological parameters are obtained for families of CDM models. For example, for COBE-normalized ΛCDM models (scalar fluctuations only), the maximum-likelihood result can be approximated by $\Omega\, n^2\, {h_{60}}^{1.3} = 0.58 \pm 0.11$. The formal random errors quoted correspond to the 90% confidence level. The total uncertainty, including systematic errors associated with nonlinear effects, may be larger by a factor of ~ 2. These results are in agreement with an application of a similar method to other data (Mark III).

Subject headings: Cosmology: observations — cosmology: theory — dark matter — galaxies: clustering — galaxies: distances and redshifts — large-scale structure of universe

1. INTRODUCTION

In the standard picture of cosmology, structure originated from small-amplitude density fluctuations that were amplified by gravitational instability. These initial fluctuations are assumed to have a Gaussian probability distribution, fully characterized by their power spectrum (PS). On large scales, the fluctuations are expected to be linear even at late times, still characterized by the initial PS. Thus, the PS is a very useful statistics for large scale-structure. We focus on the PS rather than the correlation function (*e.g.*, Górski *et al.* 1989) because the PS distinguishes more clearly between the processes that affect structure formation on different scales. It also has the advantage of being less sensitive to assumptions regarding the mean density.

The PS has been estimated from several redshift surveys of galaxies (see reviews by Strauss & Willick 1995; Strauss 1998). However, the distribution of galaxies does not necessarily provide a direct measurement of the underlying *mass* distribution; the PS estimated from redshift surveys is contaminated by unknown "galaxy biasing". Additional complications arise from redshift distortions, triple-value zones and nonlinearities of the density field. This also complicates a direct comparison of the correlation function derived from galaxy density fluctuations with similar quantities derived from peculiar velocity measurements. Therefore, it is advantageous to estimate the mass PS directly from purely dynamical data. Another advantage of velocity over density data is that they probe the density field on scales larger than the sample itself, and that they are subject to weaker nonlinear effects. It is therefore easier to obtain an approximation for the initial PS from the current velocity PS than from the current density PS.

Direct estimation of the PS from reconstructed velocity or density fields is complicated by the need to correct for the effects of large noise, smoothing, and finite and nonuniform sampling (*e.g.*, Kolatt & Dekel 1997). On the other hand, the likelihood analysis of peculiar velocities, such as the one applied here, provides an appealing method for estimating the mass PS since it is a straightforward statistic acting on the 'raw' data, without the need for processing such as binning, smoothing, or applying a full POTENT reconstruction (Dekel, Bertschinger & Faber 1990). It takes into account the measurement errors and finite discrete sampling, and it utilizes much of the information content of the data. The simplifying assumptions made in our main analysis are that the peculiar velocities are drawn from a Gaussian random field, that the velocity correlations can be derived from the density PS using linear theory, and that the errors in the measurements are Gaussian. Other limitations of the method are the need to assume some parametric functional form for the PS, with a possible sensitivity of the results to the choice of this model, and the fact that the likelihood analysis provides only relative likelihood of the different models, not an absolute goodness-of-fit.

PS estimates using likelihood analysis (Zaroubi *et al.* 1997) has been obtained from the "Mark III" catalog of peculiar velocities (Willick *et al.* 1997a), yielding relatively high values for the PS, in agreement with the direct estimates from the "POTENT" reconstruction (Kolatt & Dekel 1997). This result is still associated with large uncertainties because the sampling of the data is sparse and nonuniform, because the merging of data from several sources is nontrivial, and because the distance errors in peculiar-velocity data are relatively large. Furthermore, the uncertainty in the assumed distance errors always propagates into an uncertainty in the resultant PS because the errors add in quadrature to the PS. It is therefore important to analyze new data of certain improved qualities and to pay special attention to the error estimates.

The data analyzed in the present paper are based on the new SFI catalog of peculiar velocities of galaxies (Haynes *et al.* 1999, Wegner *et al.* 1999), containing about 1300 field spiral galaxies with Tully-Fisher (TF) distances. Most of the measurements in the SFI catalog are new. Data taken from the literature which are included in the catalog, mostly those by Mathewson, Ford & Buchhorn (1992), have been recalibrated to match the new observations both for magnitude and line width scale. This procedure should minimize the effects of combining different datasets, effects of significant concern in Mark III (e.g., Willick & Strauss 1998). The SFI catalog, though sparser than Mark III in certain places, covers more uniformly the volume out to $70\,\mathrm{h}^{-1}$Mpc.

The distances in the SFI catalog have been estimated using a linear TF relation derived from a matching cluster sample (Giovanelli *et al.* 1997a, 1997b; SCI). Possible deviations from the standard, linear TF relation were ignored since no clear evidence for such deviations was detected in the data. In addition, the sensitivity to such an effect is small because of the the selection criteria of the SFI catalog.

The crucial issue of error estimate is addressed in two ways. First, the fact that the SFI field sample is matched by the SCI cluster sample of similar size allows a careful investigation of the observational and internal scatter of the TF distances which provides a good a priori estimate of the errors. These errors are adjusted for an assumed difference in the scatter between field and cluster galaxies. An additional adjustment of the scatter is due to our bias-correction procedure.

A second and independent approach to estimate the errors is to include them as an extra parameter in the likelihood analysis so that it also determines the maximum-likelihood values for the errors. In that approach, we use a parametric model for the errors which builds upon the original estimates of width-dependent errors.

We address here the mass-density power spectrum as derived from peculiar-velocity data, with or without Cosmic Microwave Background (CMB) fluctuation data, but independent of the distribution of galaxies in redshift space. We thus determine the quantity $P(k)\Omega^{1.2}$ (where $P(k)$ is the density power spectrum and Ω is the cosmological density parameter), while we are free of assumptions regarding the "biasing" relation between galaxies and mass. We can therefore measure a purely dynamical parameter such as $\tilde{\sigma}_8 \equiv \sigma_8\Omega^{0.6}$ (where σ_8 is the rms mass-density fluctuation in top-hat spheres of radius $8\,h^{-1}$Mpc). When assuming a priori a parametric functional form for the mass PS, *e.g.*, based on a generic CDM model, we can in fact determine a combination of dynamical parameters such as Ω and the power index n.

Investigations involving galaxy redshift surveys commonly measure a different parameter that does involve galaxy biasing, $\beta \equiv \Omega^{0.6}/b$ (where b is the biasing parameter). The parameters $\tilde{\sigma}_8$ and β (at $8\,h^{-1}$Mpc) are related via σ_{8g}, referring to the rms fluctuation in the galaxy number density. A number of measurements of β have been carried out so far, either based on redshift distortions of the IRAS 1.2 Jy redshift survey (Fisher *et al.* 1995) or based on comparisons of this redshift survey and the peculiar-velocity data. Most recent velocity-velocity comparisons found values for β in the range of $0.5 - 0.7$ (Davis, Nusser & Willick 1996; Willick *et al.* 1997b; da Costa *et al.* 1998; Kashlinsky 1998; Willick & Strauss 1998), while density-density comparisons have lead to values as high as 0.9 (e.g. Sigad *et al.* 1998). A determination of $\tilde{\sigma}_8$ from the SFI data may help to clarify the situation.

In § 2 we describe the data and our method for correcting Malmquist bias. In § 3 we present the method of analysis and the parametric models used as priors. The method is tested using mock catalogs in § 4. The estimated power spectra and the constraints on the cosmological parameters are presented in § 5. The robustness of the results is addressed in § 6. We discuss our results and conclude in § 7.

2. DATA

2.1. Sample and Distance Errors

The SFI sample is based on a wide-angle survey of Sbc-Sc galaxies with I-band TF distances, covering declinations $\delta \geq -45^o$ and galactic latitudes $b \geq 10^o$. The galaxy selection criteria depend on redshift in order to ensure dense sampling at large distances; the catalog consists of three zones of different diameter limits and redshift limits. This data set was complemented south of $\delta = -45^o$ with galaxies drawn from the Mathewson *et al.* (1992) survey, carefully converted to the same system of magnitude and line-width, and with the same set of corrections and selection criteria applied to the whole sample (Giovanelli *et al.*

1997a, 1997b). The combined sample comprises of about 1300 field galaxies, extending out to 7500 $\mathrm{km\,s^{-1}}$ in redshift, and quite isotropically covering the whole sky except of the Galactic zone of avoidance.

Accurate estimation of the uncertainty Δ in the distance are important both for the bias correction (see § 2.2) and for determination of the PS (see § 3). The uncertainties are derived from the estimate of the scatter in the observed TF relation. We take advantage of the fact that the SFI sample is matched by a similar cluster sample (SCI, Giovanelli *et al.* 1997a, 1997b). The line-width dependent scatter of this cluster sample is well determined. Since SCI was observed using the same observational procedures as most galaxies in SFI, the distance estimates in both samples should suffer from similar observational uncertainties. However, it is less clear whether the intrinsic scatter of the TF relation is the same for the field and cluster samples. We have parameterized the total scatter in the SFI sample by using the SCI observed scatter and adding an additional intrinsic scatter for field galaxies in quadrature. Such a higher scatter for field galaxies has consistently been found by a number of authors (e.g. Bothun & Mould 1987; Freudling, Martel & Haynes 1991). We estimated the total scatter of SFI by taking advantage of the distance dependence of biases in the inferred distances. These biases for field galaxies are large at high distances and dominate the raw measured peculiar velocities. The exact behavior at large distance depends on the assumed amplitude of the scatter (see Freudling *et al.* 1995). With the aid of mock samples, the observed distance dependence of the average measured peculiar velocity was used to infer the intrinsic scatter for the SFI sample.

The resulting errors are estimated to be in the range $15 - 20\%$, and increasing with decreasing line-width w. Following da Costa *et al.* (1996), a small fraction ($\sim 7\%$) of galaxies with small line-width ($\log w \leq 2.25$) has been discarded because of the unreliability of the TF relation and its scatter at such line-widths. A detailed account on the sample selection, error estimates, and the procedure of combining the two datasets can be found in Wegner *et al.* (1999) and Haynes *et al.* (1999). The SCI sample of ~ 500 galaxies within 24 clusters was used for calibrating the TF relation and in estimating the scatter properties, but the peculiar velocities of these clusters themselves are not used in this work as they require a different treatment.

2.2. Bias Correction

It is crucial to properly correct the data for systematic biases, such as those arising from the coupling between the random distance errors, the geometry of space and the inhomogeneities in the underlying distribution of galaxies, and certain aspects of the sample selection. Due to the complexity of the selection criteria and the TF distance errors in the SFI data, the bias correction could not be properly estimated using the standard simple analytic expression. In earlier papers of the SFI series, the bias was estimated using a numerical Monte-Carlo approach in which the selection criteria were mimicked in detail (Freudling *et al.* 1995). Here, we replace it with a simpler semi-analytic estimate of the bias, which incorporates the relevant selection criteria.

The bias-correction method will be described in detail by Eldar *et al.* (1998). Here we mention only the basic features of the method. Given a galaxy with a TF inferred distance d and a line-width $\eta = \log w - 2.5$, the Malmquist-corrected distance is adopted to be the conditional expectation value of the true distance, r,

$$E(r|d,\eta) = \frac{\int_0^\infty dr\ r\ P(r,d,\eta)}{\int_0^\infty dr\, P(r,d,\eta)}, \tag{1}$$

where $P(r,d,\eta)$ is the joint probability distribution in the catalog (*e.g.*, Strauss & Willick 1995). The line-width is explicitly included to ensure that the correction holds when the selection criteria depend on η.

This joint distribution is derived from several input quantities. One is the underlying spatial number density of galaxies, $n(r)$, which is taken from a self-consistent real-space reconstruction from the IRAS 1.2 Jy redshift survey (as described in Sigad *et al.* 1998). Another input is the distribution of galaxy diameters, $\Phi(D)$. One also needs as input the conditional probability $P(\eta, B, I|D)$, that a galaxy with a given D will have a line-width η and absolute magnitudes B and I. We adopted the same distribution functions as those used in Freudling *et al.* (1995). Taking into account the selection in angular diameter, $a = D/r$, and the apparent blue magnitude limit $m_{B,\max}$, one obtains

$$P(r,d,\eta) \propto r^2 n(r) \int_{-\infty}^{\infty} da\ S(a|r)\ \Phi(ar)\ r\ \ \exp\left(-\frac{[\ln(r/d)]^2}{2\Delta^2}\right)\ P(r,d,\eta,ar|m_{B,\max}). \tag{2}$$

The selection function of angular diameters at a given true distance, $S(a|r)$, is derived from the corresponding selection function in redshift space, $S_z(a|z)$, via

$$S(a|r) = \int_{-\infty}^{\infty} dz\ S_z(a|z)\ P(z|r), \tag{3}$$

where $P(z|r)$ is based on the model peculiar-velocity field. The joint distribution $P(r,d,\eta,ar|m_{B,\max})$ is based on a combination of the diameter–magnitude relation, the correlation between B and I Magnitudes, the $\eta - B$ relation, and the B-magnitude limit in the selection of galaxies.

This bias correction scheme was tested, and its details were refined, using carefully constructed mock catalogs (presented below, § 4.1). We also tried several variants of the procedure to correct the real data for biases. The results of the power-spectrum analysis turn out to be fairly insensitive to the specifics of the bias correction scheme. In particular, for the underlying galaxy-density field that enters the correction via $n(r)$, we tried replacing the IRAS field (Sigad *et al.* 1998) with a linear reconstruction of a combination of IRAS and optical data (Freudling, da Costa & Pellegrini 1994), and found negligible effects on the results of the likelihood analysis.

The estimated errors in the observed TF relation can be directly translated into a distance uncertainty for each galaxy prior to the correction for biases. However, the correction for biases changes the properties of the scatter for a given location in estimated-distance space, which leads to a different uncertainty in the bias-corrected distance estimate. The semi-analytic approach is used also for a re-evaluation of the distance errors after the bias correction. We find that the bias correction acts towards slightly decreasing (by $\sim 10\%$) the average error, because of the additional information incorporated by the selection effects and the underlying density field used in the bias correction. The validity of this approach is verified using the mock catalogs (which also shows that the distribution of distance errors after the bias correction closely resembles a Gaussian distribution, Eldar *et al.* 1998). An independent verification of the magnitude of errors within the framework of the likelihood analysis is described in § 5.1. In what follows, we refer to these errors as our 'original' error estimates.

3. METHOD

3.1. Likelihood Analysis

The goal of this paper is to estimate the power spectrum of mass density fluctuations from peculiar velocities, by finding maximum likelihood values for parameters of assumed model power-spectra. Again, the underlying assumptions are that the velocities and their errors are Gaussian, and that the velocity correlations can be derived from the density PS using linear theory. The assumption regarding the Gaussianity of the velocity field is supported by simulations which show that it is Gaussian well into the quasi-linear regime (Kofman *et al.* 1994). This is farther verified for our data set by the fact that the distribution of observed $\ln(z/d)$ closely resembles a Normal distribution. The validity of the second assumption is discussed later in § 6.3.1. The likelihood analysis method is described in Zaroubi *et al.* (1997; see also Kaiser 1988; Jaffe & Kaiser 1994). Here we summarize the main ideas, the underlying assumptions, and the specific application to peculiar velocities. Given a data set $\mathbf{d}$, our objective is to estimate the most likely model $\mathbf{m}$. Using Bayes theorem

$$\mathcal{P}(\mathbf{m}|\mathbf{d}) = \frac{\mathcal{P}(\mathbf{m})\mathcal{P}(\mathbf{d}|\mathbf{m})}{\mathcal{P}(\mathbf{d})}\,, \tag{4}$$

and assuming a uniform prior $\mathcal{P}(\mathbf{m})$, this can be turned to maximizing the likelihood function, the probability of obtaining the data given the model, $\mathcal{L} = \mathcal{P}(\mathbf{d}|\mathbf{m})$, as a function of the assumed model parameters.

Under the assumption that both the underlying velocities and the observational errors are independent Gaussian random fields, the likelihood function can be written in the following form

$$\mathcal{L} = \left[(2\pi)^N \det(R)\right]^{-1/2} \exp\left(-\frac{1}{2}\sum_{i,j}^{N} u_i R_{ij}^{-1} u_j\right)\,. \tag{5}$$

This is simply the corresponding multivariate Gaussian distribution, where $\{u_i\}_{i=1}^N$ is the set of N observed peculiar velocities at locations $\{\mathbf{r}_i\}$, and R is their correlation matrix. Expressing each data point as the sum of the actual signal and the observational error $u_i = s_i + \epsilon_i$, the elements in the correlation matrix have two contributions

$$R_{ij} \equiv < u_i u_j > = < s_i s_j > + < \epsilon_i \epsilon_j > = S_{ij} + {\epsilon_i}^2 \delta_{ij}. \tag{6}$$

The first term is the correlation of the signal, that is calculated from theory. The second term is the contribution of the distance errors, which are assumed to be uncorrelated. This should be true for the observational errors and the intrinsic scatter of the TF relation. We tested the impact of uncertainties in the bias correction, which might lead to correlated errors, by varying parameters of our bias model within the expected uncertainties. The changes in the results reported below are negligible compared to other systematic and random errors. For a given PS, the signal terms are calculated using their relation to the parallel and perpendicular velocity correlation functions, $\Psi_\parallel$ and $\Psi_\perp$,

$$S_{ij} = \Psi_\perp(r)\sin\theta_i\sin\theta_j + \Psi_\parallel(r)\cos\theta_i\cos\theta_j\,, \tag{7}$$

where $r = |\mathbf{r}| = |\mathbf{r}_j - \mathbf{r}_i|$ and the angles are defined by $\theta_i = \hat{\mathbf{r}_i}\cdot\hat{\mathbf{r}}$ (Górski 1988; Groth, Juszkiewicz & Ostriker 1989). In linear theory, each of these can be calculated from the PS,

$$\Psi_{\perp,\parallel}(r) = \frac{H_0^2 f^2(\Omega)}{2\pi^2}\int_0^\infty P(k)\,K_{\perp,\parallel}(kr)\,dk\,, \tag{8}$$

where $K_\perp(x) = j_1(x)/x$ and $K_\parallel(x) = j_0 - 2j_1(x)/x$, with $j_l(x)$ the spherical Bessel function of order l. The cosmological Ω dependence enters as usual in linear theory via $f(\Omega) \simeq \Omega^{0.6}$, and H_0 is the Hubble constant.

The likelihood analysis is performed by assuming some parametric functional form for the PS. For each assumed PS, the correlation matrix R is obtained and used to calculate the likelihood function (eq. [5]). Exploring the chosen parameter space, we find the PS parameters for which the likelihood is maximized. (Note that since the model parameters appear also in the normalizing factor of the likelihood function, through R, maximizing the likelihood is *not* equivalent to minimizing the χ^2.) The main computational effort is the calculation and inversion of the correlation matrix R in each evaluation of the likelihood. It is an $N \times N$ matrix, where the number of data points N is typically more than 1000.

Since the input data are peculiar velocities, the method essentially measures the combination $f(\Omega)^2 P(k)$, and not directly the mass-density $P(k)$ by itself. This degeneracy between Ω and the PS can be broken when Ω enters explicitly into the functional form characterizing the PS shape, as in CDM models (§ 3.2).

Confidence levels are estimated by approximating $-2\ln\mathcal{L}$ as a χ^2 distribution with respect to the model parameters. The likelihood analysis provides only relative likelihoods of different models. An absolute measure of goodness-of-fit can be provided, for example, by the value of the χ^2 obtained with the parameter values associated with the maximum likelihood. A χ^2 per degree of freedom of about unity would indicate that the model provides a good statistical description of the data.

3.2. Power Spectrum Models

In order to perform the likelihood analysis, a specific parametric form for the PS is needed. For the main analysis of the paper, we use families of generalized CDM models normalized by the COBE 4-year data. The general form of these models is

$$P(k) = A_{COBE}(n, \Omega, \Lambda)\, T^2(\Omega, \Omega_B, h; k)\, k^n \,, \tag{9}$$

where A is the normalization factor and $T(k)$ is the CDM transfer function proposed by Sugiyama (1995, a slight modification of Bardeen *et al.* 1986):

$$T(k) = \frac{\ln(1 + 2.34q))}{2.34q} \left[1 + 3.89q + (16.1q)^2 + (5.46q)^3 + (6.71q)^4\right]^{-1/4} \,, \tag{10}$$

$$q = k\left[\Omega h\, \exp(-\Omega_b - (2h)^{1/2}\Omega_b/\Omega)\,(\,h\,\mathrm{Mpc}^{-1})\right]^{-1} \,. \tag{11}$$

These models include open universes with no cosmological constant, flat models with a cosmological constant ($\Omega + \Omega_\Lambda = 1$), and tilted models with a large-scale power index n that can be different from unity. The latter may include tensor fluctuations with tensor to scalar ratio of quadrupole moments of $T/S = 7(1 - n)$. The free parameters in the CDM models are Ω, h and n. In all cases the baryonic density is set to be $\Omega_b = 0.024h^{-2}$ (*e.g.*, Tytler, Fan & Burles 1996). For each model, the amplitude A is fixed by the COBE 4-year data.

We followed the COBE normalization adopted in Zaroubi *et al.* (1997), who used the COBE DMR data (Hinshaw *et al.* 1996) to set the PS amplitude calculated by different authors (Górski *et al.* 1995; Sugiyama 1995; White & Bunn 1995) for various cosmological CDM-like models. The calculation of Sugiyama (1995) was used as a reference. For models not studied by him the other results were used, after matching them to Sugiyama's in the commonly studied models. For a summary of the COBE normalization results see Górski *et al.* (1998).

In addition, we use a different parameterization of the same power spectra, namely

$$P(k) = A\,k\,T^2(k), \quad T(k) = \left(1 + [ak/\Gamma + (bk/\Gamma)^{3/2} + (ck/\Gamma)^2]^\nu\right)^{-1/\nu}, \tag{12}$$

with $a = 6.4\,\mathrm{h}^{-1}\mathrm{Mpc}$, $b = 3.0\,\mathrm{h}^{-1}\mathrm{Mpc}$, $c = 1.7\,\mathrm{h}^{-1}\mathrm{Mpc}$ and $\nu = 1.13$ (*e.g.*, Efstathiou, Bond & White 1992). In the context of the CDM model, Γ has a specific cosmological interpretation, $\Gamma = \Omega h$. Below, however, we use equation (12) as a generic form with limiting logarithmic slopes $n = 1$ and -3 on large and small scales respectively, and with a turnover at some intermediate wavenumber that is determined by the single shape parameter Γ. Hereafter, we refer to this functional form of the power-spectrum as the "Γ model". We use it as a convenient parameterization, for comparability with other works, and for relaxing the COBE normalization. The free parameters that we vary in this case are the amplitude A and the shape parameter Γ.

3.3. Error Models

We make a special effort to estimate the distance errors. As mentioned in section 1, this is done because the amplitude of the deduced PS depends on their sum in quadrature; if errors are overestimated, the PS is underestimated and vice versa.

We first apply the likelihood analysis with the original distance errors, σ_{oi}, as estimated a priori for each galaxy (i) in the SFI catalog with the procedure explained in section 2.2. Alternatively, we incorporate the errors in the likelihood analysis itself, by allowing a parametric model for the errors in addition to the parametric model of the PS. An error model is fully specified by the standard deviations σ_i because we assume that the distance errors for the individual galaxies are uncorrelated and that the scatter is Gaussian. We try two alternative global modifications of the original errors as our error model: one is based on a free multiplicative factor, $\sigma_i = p\sigma_{oi}$, and the other is based on a free additive constant in quadrature, $\sigma_i = (\sigma_{oi}^2 \pm q^2)^{1/2}$. The latter is similar to the way we modeled the difference in scatter between the field and cluster samples (see § 2.1). The errors are incorporated in the model that constitutes the correlation matrix, and the parameters p or q are adjusted simultaneously with the parameters of the PS until the likelihood is maximized.

The apparent cost of adding the error parameter to the likelihood analysis is a larger formal error in the final results for the power spectrum and the cosmological parameters. However, since our original error estimates carries some uncertainty, this procedure, which provides an almost independent estimate of the errors, could add to the overall confidence in our results.

4. TESTING THE METHOD

4.1. Mock Catalogs

It is essential to check the method with realistic mock catalogs, in view of the large errors in the data and the approximations made in the analysis. For this purpose, we use the N-body simulation of Kolatt *et al.* (1996) which was designed to mimic the large-scale density distribution in our local universe. The simulation is based on initial conditions extracted from a reconstruction of the smoothed ($5\,h^{-1}$Mpc Gaussian) real-space density field from the IRAS 1.2 Jy redshift survey, taken back into the linear regime. Small-scale perturbations were added by means of constrained random realizations, and the system was then evolved forward in time using a particle-mesh N-body code until a present epoch defined by $\sigma_8 = 0.7$. The "true" PS was calculated directly from the underlying mass distribution of the simulation, by Fourier transforming to k-space and calculating the power in bins of wavelength.

"Galaxies" were identified in the simulation via a linear biasing scheme, and then divided into galaxy types, S's and E's, while obeying the morphology-density relation. Observational parameters were assigned to the S galaxies in the mock sample according to the prescription of Freudling *et al.* (1995), and perturbed at random according to the estimated observational errors. Subsequently, we selected ten random mock SFI samples using the exact selection criteria of the real SFI sample. Each of these mock catalogs was corrected for biases, and the errors were re-evaluated accordingly, in the same way as in the real data (see Eldar *et al.* 1998).

4.2. Testing with the Γ Model

We first apply the likelihood analysis to the mock SFI catalogs using the Γ functional form (eq. [12]) as the prior model for the PS. We allow the amplitude A and the shape parameter Γ to vary, and include an additional free parameter in the error model. It is realized that the freedom provided by this family of models (just as by any other family of models) may not be enough for an adequate fit to the true PS. No additional constraint is applied on large scales, so this is a test of the ability of the velocity data alone to constrain the PS.

Figure 1 (left panel) shows a contour plot of the resulting log-likelihood ($\ln\mathcal{L}$) in the parameter plane ($A-\Gamma$), as obtained from one of the realizations of the mock catalogs. The errors in this case were allowed to vary by the multiplicative factor p, and the plot shown corresponds to the best-fit error parameter. Here, and in all the figures that follow, the log-likelihood contours are relative to the maximum likelihood with contour spacing of $\Delta[\ln\mathcal{L}]=-1$. The right panel of Figure 1 shows the corresponding best-fit power spectrum (solid line). The filled symbols mark the target of the reconstruction — the true PS of the simulation. The shaded area about the derived PS corresponds to the region of 90% confidence about the most-likely parameters in the likelihood plot, for fixed errors. The uncertainty becomes large at small k's corresponding to scales larger than the sampled volume, because no additional data were used to constrain the PS on large scales. The figure demonstrates that for this random realization the likelihood analysis with the Γ model recovers the true PS well within the error-bars. A similar quality of recovery is obtained for all the random realizations of the mock catalogs, and also when the errors are varied in the alternative way.

The maximum-likelihood errors are found to be within 5% of their "true" values. The latter were estimated by slightly modifying the known distance errors (as built into the mock catalogs) after correcting for Malmquist bias. The 5% error reflects the imperfect match between the assumed family of shapes for the PS and the true shape, and, perhaps, the uncertainty in the modification of the error estimate or the slight deviation of the modified errors from a Gaussian distribution.

4.3. Testing with a Tilted ΛCDM Model

We wish to check the success of the likelihood analysis also with the COBE-normalized CDM models. We choose as our test case the flat ($\Omega+\Omega_\Lambda=1$) ΛCDM family of models, with tensor fluctuations, a corresponding tilt in n, and a Hubble constant of $h=0.6$. COBE

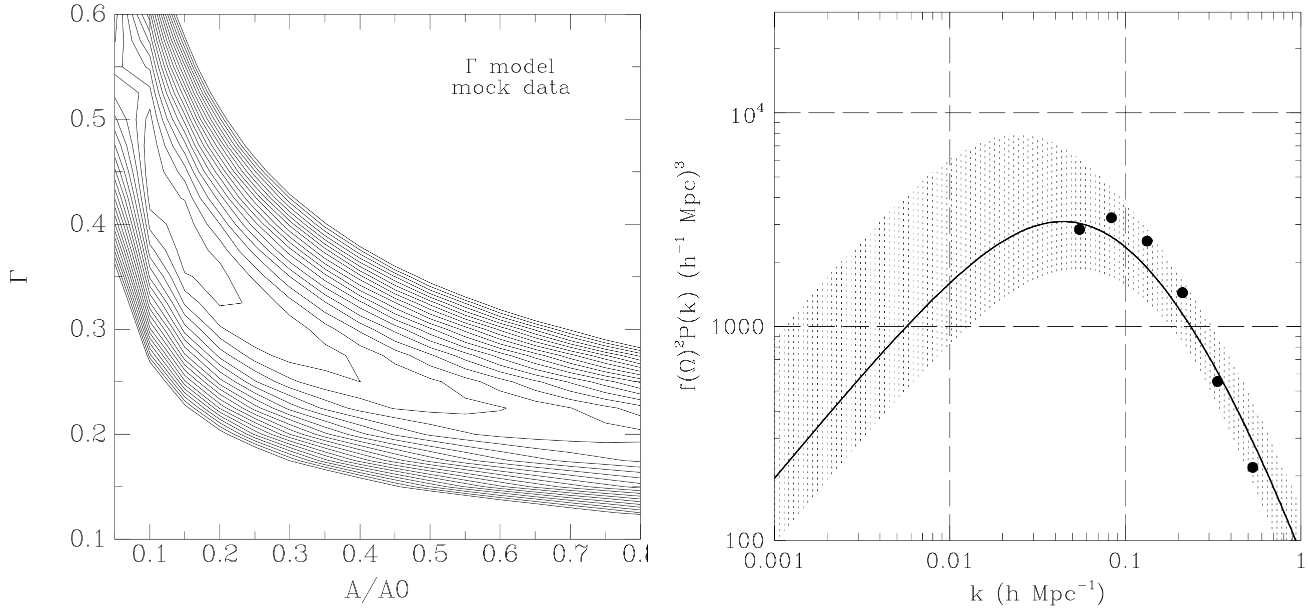

Fig. 1.— Left panel: Contour map of $\ln\mathcal{L}$ in the $A-\Gamma$ plane for one random mock catalog. Contour spacing is $\Delta[\ln\mathcal{L}] = -1$. A is in units of $A_0 = 2.0 \times 10^6(\,h^{-1}\mathrm{Mpc})^4$. The errors were varied by a multiplicative factor. Right panel: The PS corresponding to the maximum-likelihood Γ-model parameters determined for the mock catalog. The filled symbols mark the true PS of the simulation. The shaded area around the PS is the 90% confidence region for the best-fit errors, obtained from the contour map.

normalization is imposed as if the mock simulation is identical to the real universe. The likelihood analysis is thus performed by varying the parameters Ω, n and the error-parameter p or q. This family of shapes for the PS is, again, not guaranteed to provide a perfect fit to the true PS. In particular, the parameter-dependent COBE normalization is not guaranteed to give the correct amplitude, since the simulation was not explicitly constrained to produce the level of large-scale CMB anisotropies detected in the real universe.

Figure 2 (right panel) shows the best-fit power spectra of the 10 mock SFI catalogs, superimposed on the true PS. This test uses the q error parameter. The left panel shows $\ln\mathcal{L}$ contours in the $\Omega-n$ plane for one representative mock catalog, with the maximum-likelihood points for all ten catalogs marked. We see that all the maximum-likelihood points fall along the ridge of high-likelihood in the one case plotted, and are therefore moderately consistent with one another. A way to translate the likelihood contours to errors in the values of the model parameters is by assuming that, with the errors fixed, $-2\ln\mathcal{L}$ has a χ^2 distribution with two degrees of freedom. Then, the 1σ confidence level around the maximum-likelihood point is at $\ln\mathcal{L} \sim -1.15$ and the 90% confidence level is at $\ln\mathcal{L} \sim -2.3$. The fact that indeed six of the ten cases fall within the 1σ contour as determined above, and nine cases fall within the 90% confidence level, indicate that this crude error estimate is quite reasonable. The

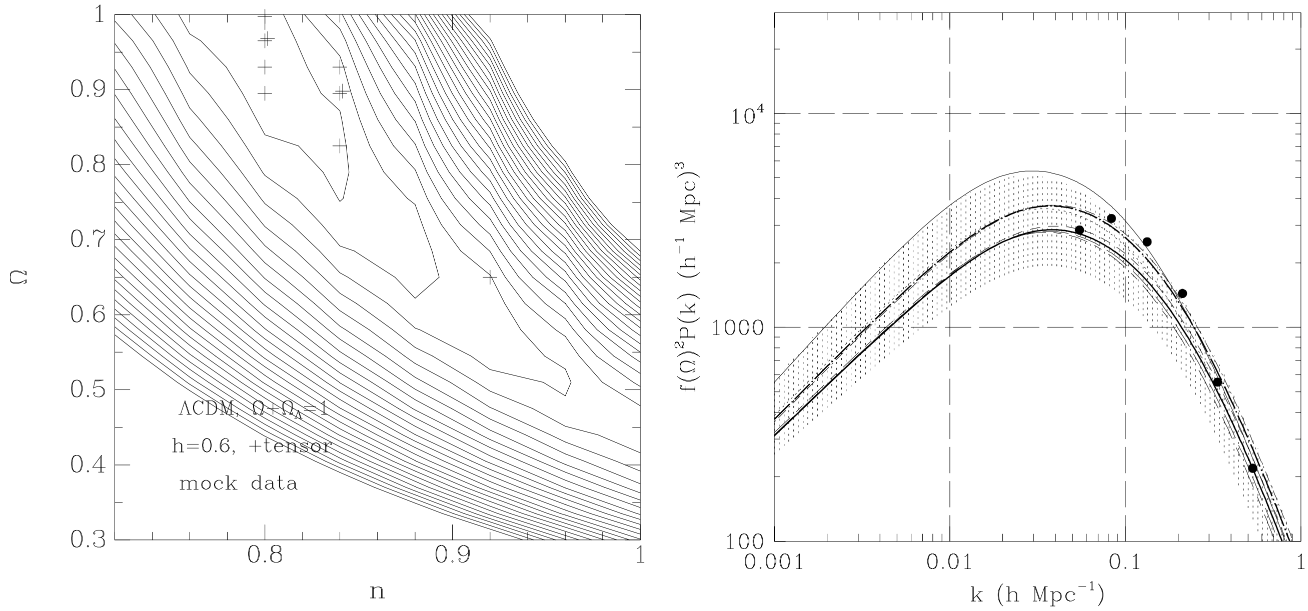

Fig. 2.— Left panel: Contour plot of ln$\mathcal{L}$ in the $n-\Omega$ plane for one of the mock catalogs, for the tilted ΛCDM model with tensor fluctuations and $h=0.6$, and the errors varied in quadrature. The best-fit values for all catalogs are marked by '+'. Right panel: Best-fit PS of the 10 mock catalogs (thick lines representing same curves derived for two different catalogs). The shaded area represents the 90% confidence region for the catalog whose contour plot is shown. The filled symbols mark the true PS of the simulation.

90% confidence region for this specific catalog is again drawn as a shaded area in the PS plot; one can see that this region indeed resembles the actual scatter of the ten cases.

The maximum-likelihood power-spectra fit reasonably well the true PS, with a fairly small spread on small and intermediate scales. For large scales (small k's) the scatter is somewhat larger, but not as large as for the Γ model which was completely free at large scales. Again, the success of recovery is similar when the alternative error parameter is used, and the errors are similar to those obtained in the case of the Γ model. It is encouraging to note that the recovery of the PS is fairly robust on the relevant scales ($k \sim 0.1\, h\, \mathrm{Mpc}^{-1}$) among the realizations, and independent of the prior model assumed for the PS, or the assumed error model.

5. RESULTS

5.1. Maximum-Likelihood Errors

Before estimating the PS from the actual SFI data, we investigate the reliability of our observational error estimate by allowing certain freedom in the errors. As a test case we use

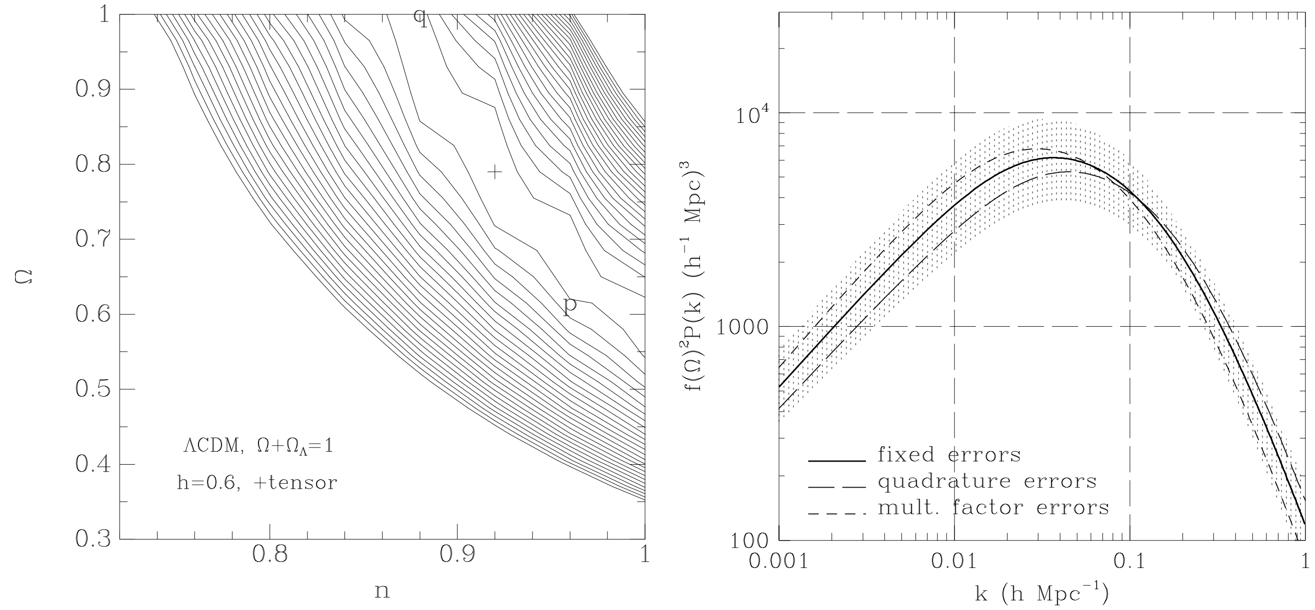

Fig. 3.— Left panel: Contour plot of ln$\mathcal{L}$ in the $\Omega - n$ plane for the SFI sample, for the tilted ΛCDM model with tensor fluctuations and $h = 0.6$, using the original error estimates. The best-fit point is marked with a '+'. The maximum likelihood locations when varying the errors in quadrature ('q') or by a multiplicative factor ('p') are also marked. Right panel: The most-likely PS for this model, for these three variants of the errors. The dotted region around the PS represents the 90% confidence limit for the case of the original errors (thick line), obtained from the high-likelihood ridge shown in the contour map.

as a prior for the PS the COBE-normalized ΛCDM family of models, with tensor fluctuations and a corresponding tilt in n, and with the Hubble constant fixed at $h = 0.6$. We perform the likelihood analysis on the real SFI data varying Ω and n, with the errors treated in three different ways; first with the errors fixed at their original values, and then by varying them according to the two error models discussed above.

Figure 3 summarizes the results obtained in these cases. The left panel shows the ln−likelihood contours in the $\Omega - n$ plane for the case of fixed errors, with the best-fit points for the three cases marked. The corresponding power spectra are presented in the right panel. In the p case, the preferred errors are 5% larger than the original ones, while in the q case the preferred errors are smaller by 0.03 in quadrature (typically a decrease of $\sim 2\%$).

The different trends in the likely errors reflect our uncertainty of the exact form of the error model. We note that while these changes are in opposite directions, they are of small magnitude, within the uncertainty expected based on the mock catalogs. The corresponding changes in the best-fit parameters are along the ridge of high likelihood in the $\Omega - n$ plane, within the 1σ confidence level, *i.e.*, it is hardly significant. In all three cases, $\chi^2/N_{dof} \sim 1$ for the best-fit PS (1.02 for the original, fixed errors, 0.99 for the p error model and 1.02 for the q error model), implying that all are reasonable fits to the data. Similar results concerning the errors are obtained when the other PS models are used as priors. The error estimate is robust to variations in the original errors about which the error model is perturbed. This likelihood analysis of the errors thus provides a very encouraging indication that the original error estimates in SFI are accurate to better than 5%. Note that "original" here refers to the refined SFI errors after the correction for biases (§ 2.2). The fact that the likelihood analysis and the semi-analytic correction converge to the same error estimate is encouraging. Based on this finding, we perform the rest of the analysis in this paper using fixed errors at their original values.

5.2. COBE Normalized CDM Models

We now use the generalized CDM families of cosmological models of the form described in equations (9) and (10). Our models include open CDM (OCDM), flat models with a cosmological constant, and tilted models with or without tensor fluctuations, allowing for variations in the cosmological parameters Ω, h, and n. For each specific choice of model and parameters the amplitude is fixed according to the 4-year COBE normalization.

5.2.1. Scale-Invariant Models

Figure 4 shows the resulting likelihood contours for the scale-invariant case, $n = 1$, for the OCDM model and the ΛCDM model. The contours are plotted in the $\Omega - h$ plane. The best-fit parameters in each case are marked, but it is clear from the elongated contours that the two parameters are not determined separately. The high-likelihood ridges rather constrain a degenerate combination of these parameters, which can be roughly fitted by the following functions:

$$\Omega\, {h_{60}}^{0.9} \;=\; 0.68 \pm 0.06\,, \qquad \mathrm{OCDM}\,; \tag{13}$$

$$\Omega\, {h_{60}}^{1.3} \;=\; 0.59 \pm 0.07\,, \qquad \Lambda\mathrm{CDM}\ . \tag{14}$$

The error-bars (here, and throughout the paper) arise from the joint 90% confidence region of the parameters. The constraints on $\sigma_8 f(\Omega)$, obtained by integrating over the corresponding power spectra, are $0.83^{+0.07}_{-0.11}$ and $0.81^{+0.13}_{-0.07}$ for OCDM and ΛCDM respectively. The error-bars quoted are the marginalized 1-dimensional 90% confidence limits. For an assumed value of h, *e.g.*, $h = 0.6$, the maximum-likelihood values are $\Omega = 0.67 \pm 0.05$ for OCDM and $\Omega = 0.58 \pm 0.06$ for ΛCDM (as marked on the plots). The $\chi^2/N_{\rm dof}$ for the best-fit PS are 1.01 and 1.04 respectively, with similar values along the high-likelihood ridge. With

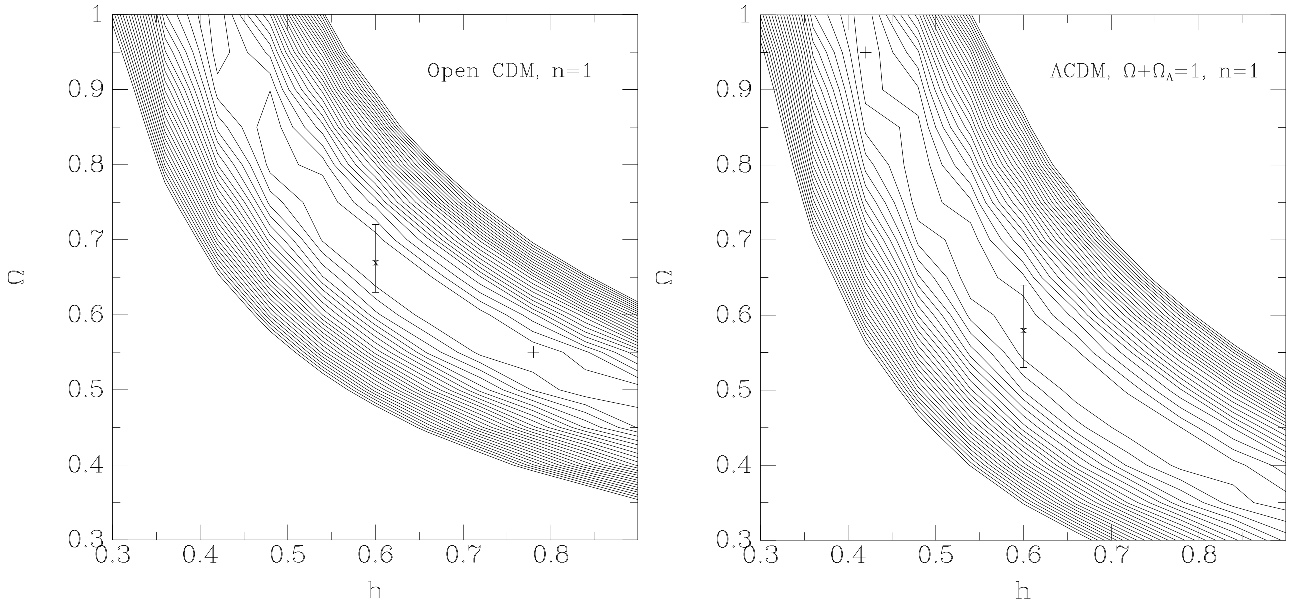

Fig. 4.— Contour plot of $\ln\mathcal{L}$ in the $\Omega - h$ plane for scale-invariant OCDM model (left panel) and ΛCDM model (right panel). The most-likely value of Ω and its 90% error bar are marked for a fixed value of $h = 0.6$.

$N_{\rm dof} = 1213$, one expects for a good fit 1.00 ± 0.04, so our CDM models indeed provide good fits to the data.

5.2.2. Tilted Models

Figure 5 presents the results obtained when allowing for a tilt in the PS on large scale relative to $n = 1$, both for the OCDM and ΛCDM families of models. The first cases considered are with scalar fluctuations only, $T/S = 0$. We fix the Hubble constant here at $h = 0.6$ while varying Ω and n. Again, the elongated ridge of high-likelihood determines a certain degenerate combination of the parameters, which can be approximated by:

$$\Omega\, n^{1.4}\, ({h_{60}}^{0.9}) \;=\; 0.68 \pm 0.07\,, \qquad \text{OCDM}\,; \tag{15}$$
$$\Omega\, n^{2.0}\, ({h_{60}}^{1.3}) \;=\; 0.58 \pm 0.08\,, \qquad \Lambda\text{CDM}\;. \tag{16}$$

The h dependence is determined for the $n = 1$ case. The corresponding constraints are $\sigma_8 f(\Omega) = 0.83^{+0.08}_{-0.10}$ for the tilted OCDM case and $\sigma_8 f(\Omega) = 0.82^{+0.10}_{-0.09}$ for tilted ΛCDM . The $\chi^2/N_{\rm dof}$ values are 1.02 in both cases, again a good fit.

The case of the tilted ΛCDM family of models, with $h = 0.6$ and with a tensor component of $T/S = 7(1-n)$, was partly discussed already as our default case in § 5.1. The likelihood map in Figure 3 reveals the familiar situation of a high-likelihood ridge that

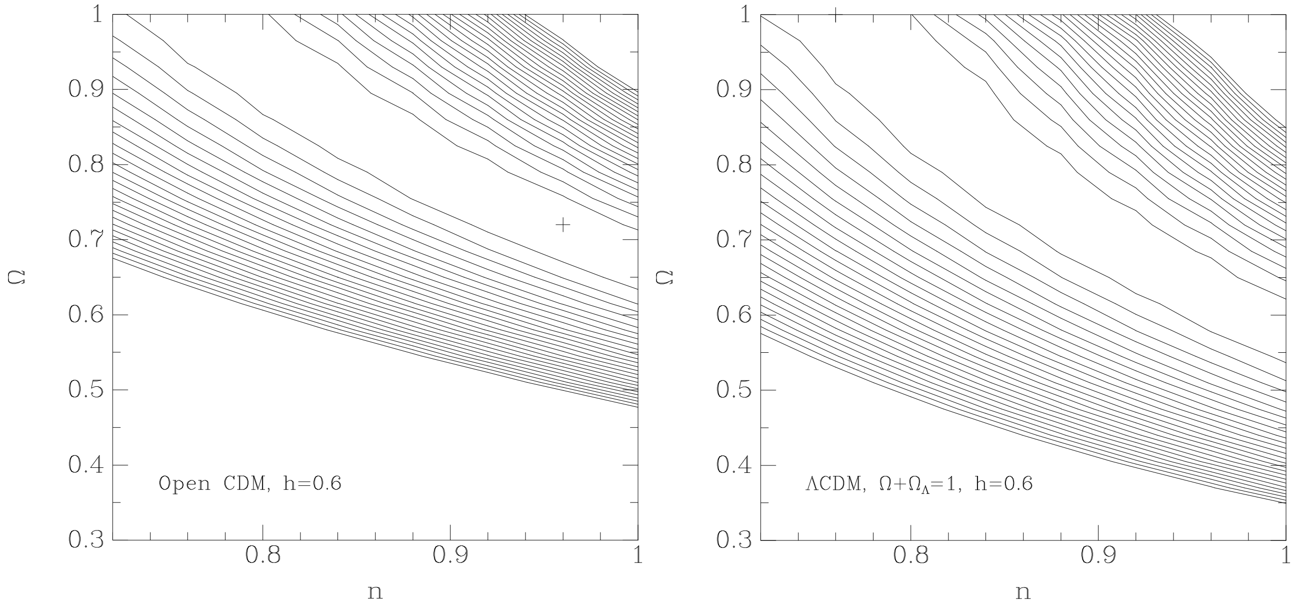

Fig. 5.— Contour plot of ln$\mathcal{L}$ in the $\Omega - n$ plane, for the tilted OCDM model (left panel) and tilted ΛCDM model (right panel). In both cases $h = 0.6$ and no tensor component is included.

constrains a degenerate combination of the cosmological parameters, now approximated by

$$\Omega\, n^{3.9} (h_{60}{}^{1.3}) \;\; = \;\; 0.58 \pm 0.08 \, , \qquad \Lambda\text{CDM } + \text{tensor} \, . \qquad (17)$$

The h dependence is determined for $n = 1$. The corresponding value of $\sigma_8 f(\Omega)$ is $0.81^{+0.09}_{-0.08}$. The uncertainty associated with the PS, shown as the shaded area in the right panel of Fig. 3, is similar to the uncertainty in the other COBE-normalized CDM variants.

5.3. Γ Model

Finally, we use the Γ model as a prior for the PS, varying the amplitude A and shape parameter Γ with no additional constraints imposed at large scales. Figure 6 shows the contours of ln$\mathcal{L}$ in the $A - \Gamma$ plane, and the corresponding best-fit PS. The maximum likelihood values are $\Gamma = 0.375 \pm 0.14$ and $A = 5.0 \times 10^5 (\,\mathrm{h}^{-1}\mathrm{Mpc})^4$. The χ^2 per degree of freedom for the maximum likelihood parameters is $\chi^2/N_{\rm dof} \; = \; 1.03$, indicating that this is a good fit to the data. The constraint obtained by integrating over the power spectra is $\sigma_8 f(\Omega) \, = \, 0.80^{+0.09}_{-0.08}$. The scatter at small k's is larger than in the case of the COBE-normalized models, due to the amplitude freedom, as seen already in the mock catalogs.

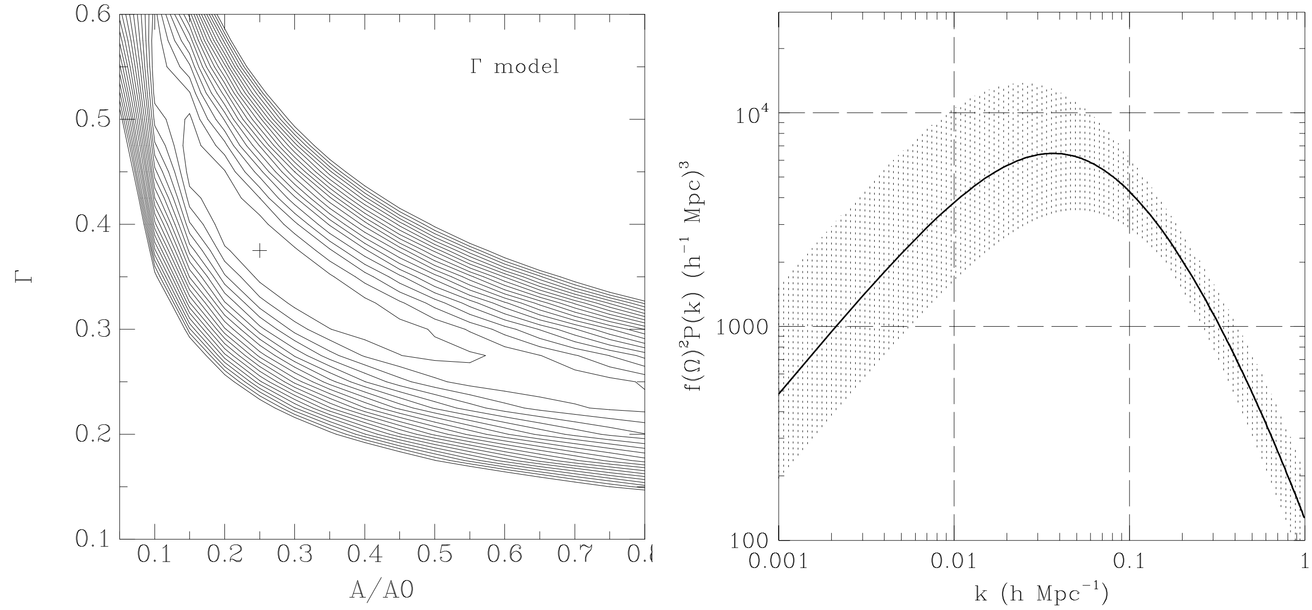

Fig. 6.— Left panel: Contour plot of ln$\mathcal{L}$ for the Γ model. The best-fit point is marked with a '+'. Right panel: The best-fit PS, with the shaded area marking the uncertainty based on the 90% confidence region of the likelihood contours.

6. ROBUSTNESS OF RESULTS

The error estimates in the parameters given in the previous section are formal 90% confidence levels. In this section, we test the robustness of these results to various variations in the data and models used.

6.1. Robustness to Models

Figure 7 shows the power spectra corresponding to the maximum-likelihood parameters for all the models presented so far in this paper, including the COBE-normalized CDM variants and the Γ model. The 90% confidence region for the tilted ΛCDM model with tensor fluctuation and $h = 0.6$ is drawn as well, as a reference for the uncertainty associated with each model based on the likelihood contours. The similarity of all the curves is striking; they agree well within the formal uncertainties of each other. The agreement is excellent for $k > 0.1$, on the scale where the data constrain the models effectively. The difference between the curves shows a slightly larger scatter on larger scales, not properly sampled by the present data. The similarity of the results using as priors the COBE-normalized CDM models and the amplitude-free Γ model indicates that the peculiar velocity data themselves contain meaningful information to constrain the PS.

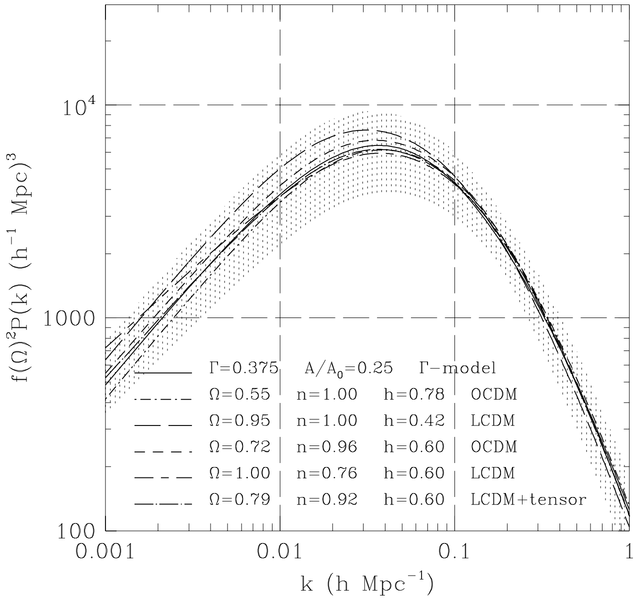

Fig. 7.— The maximum-likelihood power spectra based on the Γ model (solid line) and the various COBE-normalized CDM models. The shaded area is once again the 90% confidence region for the tilted ΛCDM model with tensor fluctuations and $h = 0.6$.

Table 1 summarizes the features of the most likely power spectra based on the various prior models. The approximate constraint on the combination of cosmological parameters as obtained from the high-likelihood ridge is given for each case. The best-fit values of the individual cosmological parameters are also listed, but recall that they carry large uncertainties. The exact location of the maximum-likelihood point in the high-likelihood ridge is hardly significant. Parameters that were held fixed in the likelihood analysis are marked in brackets. Several characteristics of the best-fit power spectra are listed: the value of $\sigma_8 f(\Omega)$, the amplitude of $f(\Omega)^2 P(k)$ at $k = 0.1\,\mathrm{h}^{-1}\mathrm{Mpc}$ and the location of the PS peak, k_{peak}. The error-bars quoted in the header represent the typical 90% confidence uncertainty in these quantities within each family of models.

The typical results for the PS are $P(k = 0.1\,h\,\mathrm{Mpc}^{-1})\Omega^{1.2} = (4.4 \pm 1.5) \times 10^3\,(h^{-1}\mathrm{Mpc})^3$ and $\sigma_8\Omega^{0.6} = 0.82 \pm 0.10$. The variations from model to model are much smaller than the formal errors for each model, increasing the above errors to 1.7 and 0.12 respectively. These results are thus almost independent of the model, at least for the family of models considered here. The actual likelihood values of all the best-fit models are very similar, and all have comparable $\chi^2/N_{dof} \simeq 1$ values. The variation of the high-likelihood ridge between the ΛCDM and OCDM families of models is more noticeable. The general constraint on the combination of cosmological parameters can be roughly approximated by $\Omega\, n^{\nu}\, {h_{60}}^{\mu} = 0.62 \pm 0.15$, where the error includes the formal uncertainties of the three parameters and the variations between models. For ΛCDM , $\mu = 1.3$ and $\nu = 2.0, 3.9$ without and with tensor

Table 1: Maximum-Likelihood Results for the various models

COBE-normalized CDM models

CDM Model	High Likelihood Ridge	$\sigma_8\Omega^{0.6}$ (± 0.10)	$P_{0.1}\Omega^{1.2}$ $(h^{-3}Mpc^3)$ (± 1500)	k_{peak} $(hMpc^{-1})$ (± 0.01)	Ω	n	h	$\chi^2/N_{\rm dof}$	$-\ln\mathcal{L}$
Open, n=1	${\Omega h_{60}}^{0.9} = 0.68 \pm 0.06$	0.83	4400	0.038	0.55	(1)	0.78	1.01	8579.4
Λ, n=1	${\Omega h_{60}}^{1.3} = 0.59 \pm 0.07$	0.81	4600	0.031	0.95	(1)	0.42	1.04	8580.1
Tilted-Open	$\Omega n^{1.4} = 0.68 \pm 0.07$	0.83	4600	0.035	0.72	0.96	(0.6)	1.02	8579.5
Tilted-Λ	$\Omega n^{2.0} = 0.58 \pm 0.08$	0.82	4200	0.037	1.00	0.76	(0.6)	1.02	8579.6
Tilted-Λ +tensor	$\Omega n^{3.9} = 0.58 \pm 0.08$	0.81	4300	0.037	0.79	0.92	(0.6)	1.02	8579.5
Γ model	$\Gamma = 0.375 \pm 0.14$	0.80	4300	0.037				1.03	8579.3

fluctuation respectively. For OCDM , without tensor fluctuations, the powers are $\mu = 0.9$ and $\nu = 1.4$.

The similarity of the power spectra obtained using the COBE-normalized CDM models and the COBE-free Γ model (see Table 1) indicates that the PS is predominantly determined by the velocity data. Therefore, we have so far ignored the error associated with the COBE normalization. As a test for the sensitivity to this error, we have repeated the analysis using the tilted ΛCDM model (with tensor fluctuations), but now normalized alternatively $\sim 18\%$ higher or lower then the mean COBE values (in accordance with the relative $\pm 1\sigma$ uncertainty associated with $Q_{rms-PS|n=1}$, Bennett *et al.* 1996). This results in a slight shift of the high-likelihood ridge, corresponding to a $\sim 6\%$ change in the constraint on the combination of parameters (eq. [17]; a smaller value is obtained for the higher normalization and vice versa), which is within our formal 1σ error-bars. However, the combined effect of the different amplitude and corresponding cosmological parameters on the PS is essentially negligible, with $\sigma_8\Omega^{0.6}$ varying by only 0.01.

6.2. Zero-point Uncertainty

A fundamental freedom in the measured peculiar velocities is in the global zero-point of the TF relation, which fixes the distances at absolute values (in km s^{-1}). Changing the

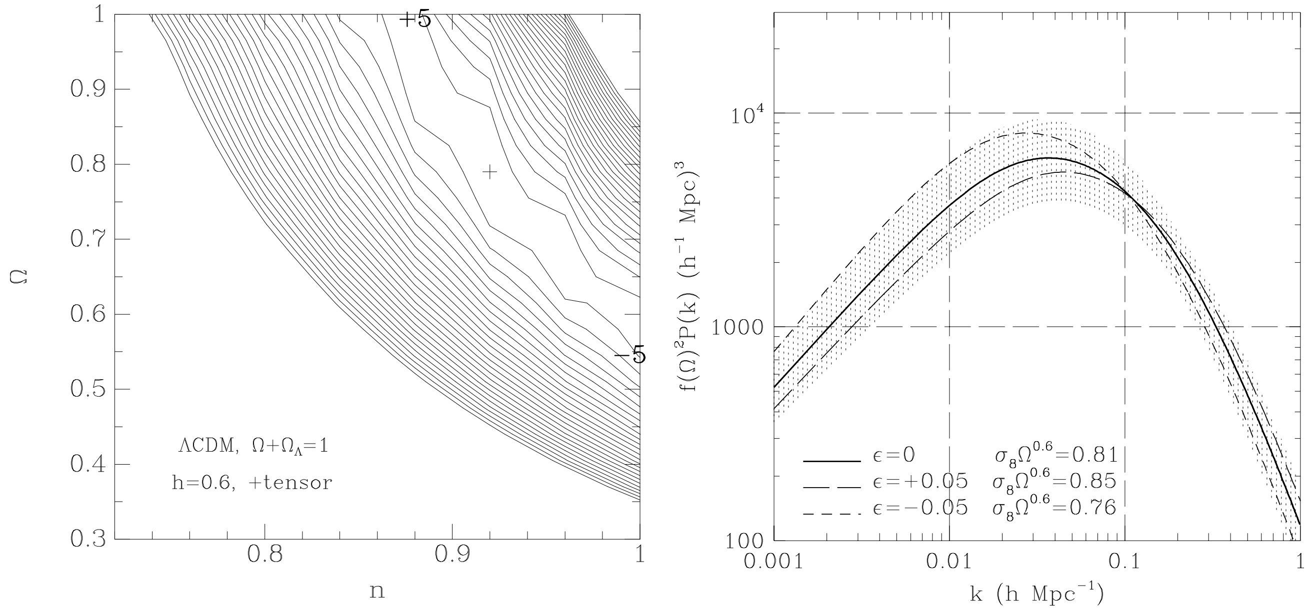

Fig. 8.— Left panel: Contour plots in the $\Omega - n$ plane for the tilted ΛCDM $h = 0.6$ model with a tensor component, for the original calibration. The maximum-likelihood point is marked by '+'. The maximum-likelihood values when varying the global zero-point by a $\pm5\%$ Hubble flow are marked by '+5','-5' accordingly. Right panel: The most likely PS for the original zero-point calibration (solid line) and when varying the zero-point by $\epsilon = +0.05$ (long dashed line) and -0.05 (short dashed line). The corresponding $\sigma_8\Omega^{0.6}$ values are marked on the plot. The shaded region is the formal likelihood 90% confidence region for the original case.

zero-point, that is multiplying the distances r by a factor $(1 - \epsilon)$, is equivalent to adding a monopole Hubble-like flow ϵr to the peculiar velocities. The zero-point calibration of the TF relation used for the SFI sample was obtained from the SCI catalog of ~ 500 galaxies within 24 clusters, using the "Basket of Clusters" approach (Giovanelli *et al.* 1997a, 1997b). The uncertainty in the zero point was estimated to be about 0.05 magnitudes, which corresponds to an uncertainty in the velocity field of 2.5% of the distance.

To estimate the effects of such uncertainties we have run the likelihood analysis with our tilted ΛCDM test-case, conservatively using zero-point changes of twice the estimated uncertainty, $\epsilon = \pm0.05$. Figure 8 illustrates the effect on the results for these cases. The changes of zero-point appear to shift the location of the maximum-likelihood values essentially along the high-likelihood ridge. The high ridge is not altered by much when the zero point varies in this range. The right panel shows the resulting best-fit PS for the three different zero points, and lists the corresponding values of $\sigma_8\Omega^{0.6}$. While the variations in the zero-point systematically affect the PS, the changes are not large; they fall within the range of the formal likelihood errors, and are of the same order of the uncertainty associated with the random distance errors (compare to Fig. 3). It is encouraging that the amplitude of the PS on intermediate scales ($k \sim 0.1\,h\,\mathrm{Mpc}^{-1}$) is robust vis-a-vis changes in in the zero point. Similar results were obtained when using the other families of PS prior models.

Similar to the uncertainty in the zero point of the distance indicator, there is also an uncertainy associated with the slope of the TF relation. This could lead to correlated errors in the inferred distances and peculiar velocities, due to the fact that the average linewidth of SFI galaxies slightly depends on distance (Wegner *et al.* 1999). However, the impact of this uncertainty on our results is even slightly smaller than that of the uncertainty in the zero point, perhaps because the SFI sample has been selected intentionally to minimize the distance dependence of the line widths.

6.3. Nonlinear Effects

A basic assumption in our analysis has been that linear gravitational instability theory is adequate for the purpose of recovering the PS from observed velocities on the scales of interest here. This is based on the fact that in the mildly-nonlinear regime the velocity field is approximated by linear theory better than the density field (basically because the velocity is a spatial integral of the density and is affected by fluctuations on larger scales). Indeed, the success of the recovery of the PS from the mock catalogs leads us to believe that this assumption is justified. However, one cannot rule out the possibility that some nonlinear effects are artificially reduced to some degree in the particle-mesh N-body simulation, and it is possible that the smooth shape of the linear PS as predicted for the CDM family of models may fail to properly match the nonlinear features that may be present on small scales in the real data. Therefore, we discuss in this section possible nonlinear effects, which could manifest themselves in different forms. For example, as coherent motions associated with the non-linear evolution of the PS (§ 6.3.1), or as incoherent random motions, perhaps due to shell-crossing, which may be modeled as an additional velocity component of dispersion σ_v (§ 6.3.2).

6.3.1. Nonlinear Power Spectra

A way to include more properly nonlinear effects in our analysis is by developing an approximation for the nonlinear evolution of the PS and then incorporating it in the likelihood analysis. Such approximations exist for the density power spectrum, P_δ (*e.g.*, Peacock & Dodds 1994; Jain, Mo & White 1995; Peacock & Dodds 1996, hereafter PD), but we need a similar approximation for the evolution of the *velocity* power spectrum, P_v, which is the quantity we actually confront with the data. A development and application of such an approximation is beyond the scope of the present paper and will be presented later (Zehavi *et al.* 1999). Here, we summarize some relevant issues and illustrate the magnitude of such effects.

Figure 9 shows the velocity PS computed in several different ways from an adaptive P^3M cosmological N-body simulation with a resolution higher by an order of magnitude than the simulation used in the present paper for the mock catalogs (but inside a smaller box of size $85\,h^{-1}$Mpc; GIF simulation, Colberg *et al.* 1999). The initial model used for P_δ is the so-called τCDM model with $\Omega = 1.0$, $h = 0.5$ and a modified shape parameter $\Gamma = 0.21$. The figure clearly demonstrates that the velocity PS is reproduced by linear theory much better than the density PS. The P_v that is computed directly from the evolved velocity field of the simulation (solid dots) lies slightly below the P_v obtained from the assumed P_δ using linear theory ($P_v \propto k^{-2} P_\delta$, solid line). On the other hand, the nonlinear correction to P_δ (*e.g.*, PD) is larger than that of P_v and in the opposite direction (upwards, as can be seen by the open dots and dashed line in Fig. 9).

One might have naively expected that the likelihood analysis using a pure linear treatment would be inferior to incorporating a non-linear correction for P_δ followed by a linear translation to P_v. However, as illustrated in Figure 9, this is not the case. The latter procedure overestimates the nonlinear effects on the velocity PS and increases the bias in the results. A similar bias is reproduced when using the mock catalogs from the low-resolution simulation of Kolatt *et al.* (1996), which exhibits a similar behavior as in Fig. 9. This could be remedied, in principle, by incorporating the evolved P_δ and then counter-balancing it with a proper approximation for the nonlinear velocity–density relation, but this would be risky as we would be applying two large corrections in opposite directions to mimic a small net effect. Until we develop a direct nonlinear correction for P_v, we adopt the fully linear procedure as our best approximation. This is justified by its success in the mock catalogs and by the expectation for only small nonlinear effects in P_v.

6.3.2. Random Motions

We have made an ad-hoc attempt to model non-linearities by introducing an uncorrelated velocity component of constant dispersion σ_v, that adds a free term at zero-lag to the correlation function derived from the linear PS model. This may be a crude way to represent small-scale random motions that are associated with multi-streaming. An alternative interpretation of this additional parameter may be as an unrecognized uncertainty in the distance estimate which does not depend on distance and is therefore not included in our usual error model. In either case, this provides a test for the robustness of our results

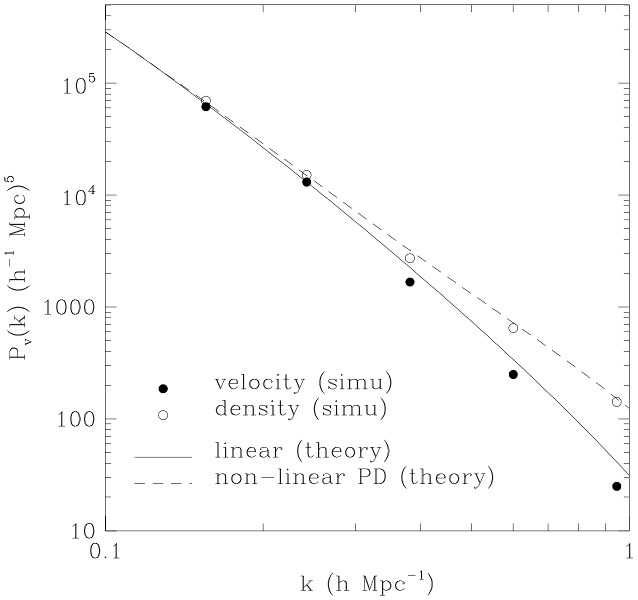

Fig. 9.— The velocity PS as computed from the high-resolution simulation of Colberg *et al.* (1999) (solid dots), compared with the theoretical linear PS (solid line), the corrected PS using the PD formalism (dashed line) and a computation via the density PS of the simulation (open dots). The latter three have been transformed to velocity PS using the linear velocity–density relation.

to an additional degree of freedom.

Figure 10 demonstrates the effect of including a free σ_v in the likelihood analysis, again for our tilted ΛCDM test-case. When allowing for this extra freedom, the preferred value turns out to be $\sigma_v = 200 \pm 120$ km s^{-1}, and is associated with a PS that is slightly lower for $k > 0.1$ and somewhat higher at small k. The value of $\sigma_8 \Omega^{0.6}$ is reduced by 14%. The deviations, in general, are comparable to the formal likelihood 90% uncertainty marked by the shaded area. The likelihood contours are somewhat sparser in this case, because of the additional scatter that reduces the sensitivity to variations in the parameters. The ridge of high likelihood is slightly shifted toward smaller values of the cosmological parameters and it can now be roughly described by

$$\Omega\, n^{3.9} ({h_{60}}^{1.3}) \;=\; 0.49 \pm 0.09\,, \tag{18}$$

a $\sim 15\%$ decrease compared to equation (17), which is of the order of the random error.

Such a preference for a non-zero σ_v associated with a change in the PS is not recovered in the mock SFI catalogs, for which a similar likelihood analysis turns out to prefer a negligible σ_v and a negligible effect on the PS. N-body simulations of higher resolution may clarify this situation.

We note that the inclusion of a free σ_v in the fit to the real SFI data leads to results

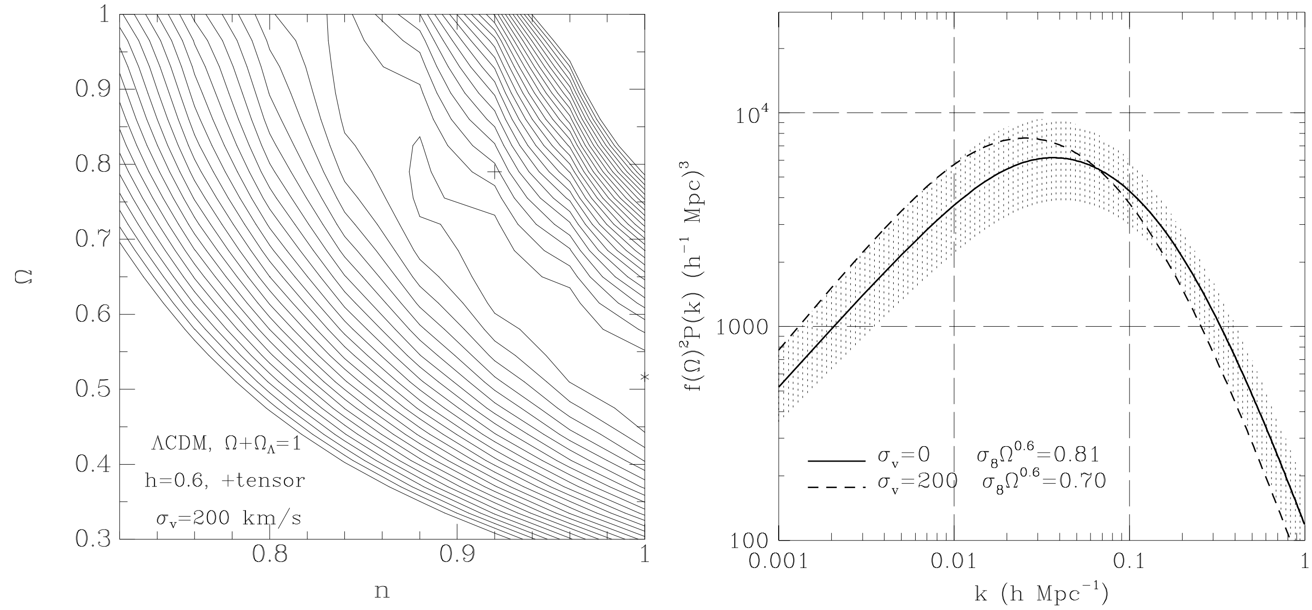

Fig. 10.— Left panel: Likelihood contour plot in the $\Omega - n$ plane for the tilted ΛCDM $h = 0.6$ model with tensor fluctuations, with an additional scatter of $\sigma_v = 200 \text{ km s}^{-1}$. The maximum-likelihood point is marked by '$*$', and the corresponding point for $\sigma_v = 0$ is marked by '+'. Right panel: The most likely PS when including $\sigma_v = 200$ in the fit (dashed line) and for the original $\sigma_v = 0$ case (solid line) together with its 90% confidence region shaded.

similar to those obtained when including a free multiplicative parameter in the error model (§ 5.1). The interpretation of a nonzero σ_v is thus not unique: It may refer to nonlinear effects that exist in the real data but not in the current simulation, or it may indicate that the actual errors are slightly larger than the original estimates. Since there is no clear benefit from adding this extra parameter and the theoretical justification as a model for nonlinear effects is weak, its inclusion in our main-stream analysis does not seem to be justified. Still, in our total error-balance, we consider a systematic error of 15% due to non-linear effects.

6.4. Comparison to the PS from Mark III

A similar likelihood analysis (though with errors fixed a priori) has been recently applied by Zaroubi *et al.* (1997) to the Mark III catalog of peculiar velocities. (Willick *et al.* 1995; 1996; 1997a). It is interesting to investigate whether the recovered power spectra are consistent with each other, given the respective uncertainties. This is intriguing because there are certain differences in the velocity fields as reconstructed from the two samples, especially in the bulk flows both in the very local neighborhood and of outer shells (*e.g.*, da Costa *et al.* 1996; 1998; Dekel 1998; Dekel *et al.* 1998; Giovanelli *et al.* 1998a, 1998b).

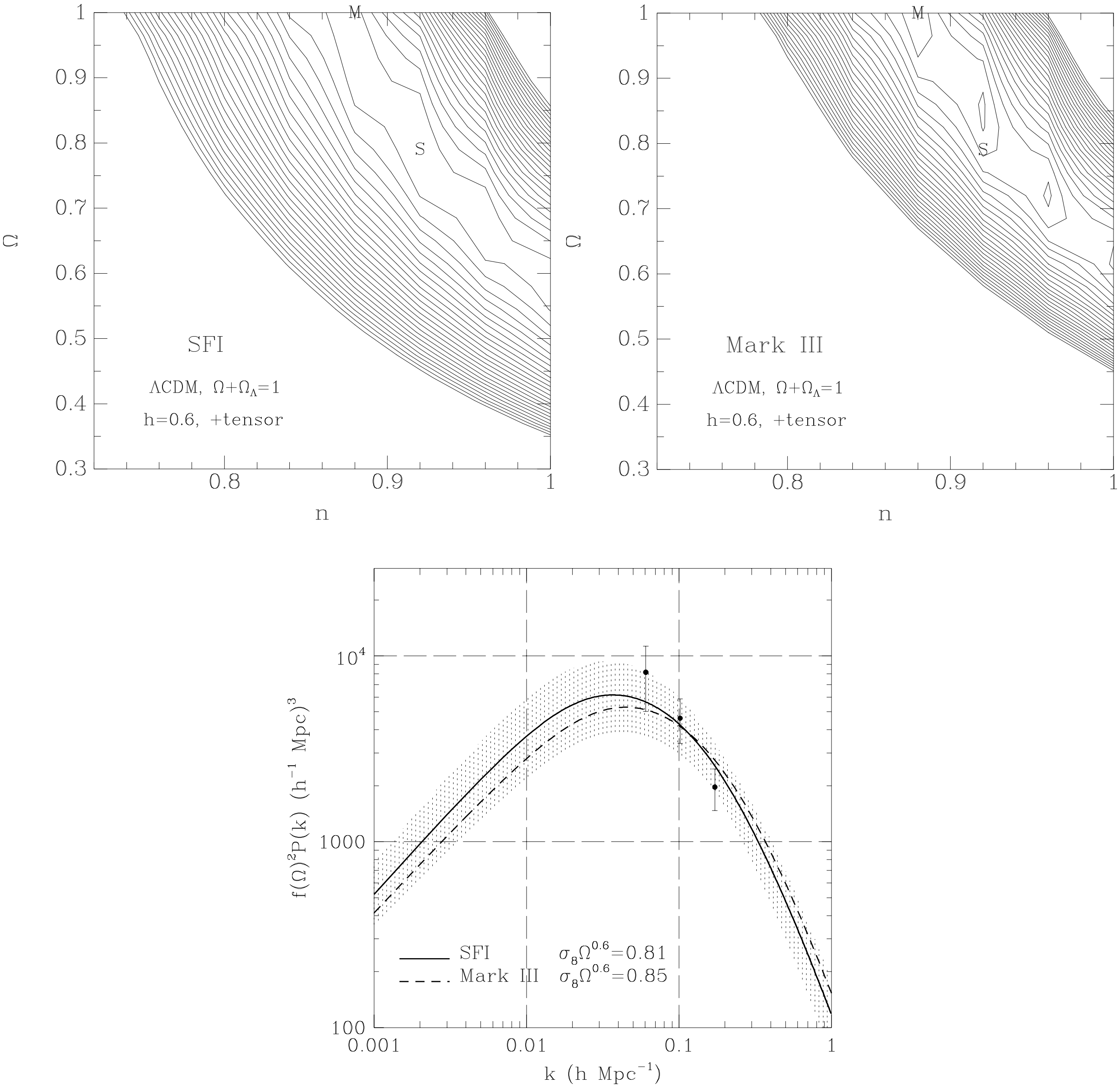

Fig. 11.— Comparison of SFI PS results to Mark III for the tilted ΛCDM test-case. Top left panel shows ln$\mathcal{L}$ contours for the SFI data, top right panel shows the contours for the Mark III data. The best-fit parameters for SFI and Mark III are marked, on both, by 'S' and 'M' respectively. The lower panel shows the maximum likelihood PS corresponding to SFI (solid) and Mark III (dashed). The 3 solid dots mark the PS calculated from Mark III by Kolatt and Dekel (1997), together with their estimated 1σ error-bar. The shaded region is the SFI likelihood 90% confidence region.

Figure 11 presents a comparison of the likelihood analysis for the two samples using our representative tilted ΛCDM family of models. Shown once again are the likelihood contours for the SFI data, together with the corresponding plot for the Mark III data. The high-likelihood ridge is similar for both samples. While the Mark III result slightly favors higher values of Ω and lower values of n, the differences are along the ridge of maximum likelihood and are therefore hardly significant. The contours are slightly more concentrated for the Mark III catalog because it consists of more galaxies.

The best-fit PS for the two catalogs are shown in the bottom panel of Figure 11, on top of the shaded area which marks the 90% confidence region for SFI. The resultant power spectra are consistent within the errors, and they agree particularly well on intermediate scales, where the data provides the most meaningful constraints. The corresponding best values for $\sigma_8\Omega^{0.6}$ are 0.81 and 0.85 for SFI and Mark III respectively. Similar results are obtained when comparing likelihood analysis of the two catalogs using the other PS models. It is worth noting here that the systematics discussed in the previous sections, with regard to the SFI analysis, are found to affect the Mark III likelihood analysis in a similar way. The PS computed by Kolatt & Dekel (1997) from the Mark III smoothed density field recovered by POTENT is also displayed on the figure (as three symbols with error bars). The agreement of the SFI result with this independent calculation of the Mark III PS is good.

A recent comparison of Mark III with IRAS 1.2 Jy (Willick & Strauss 1998) suggests an alternative zero-point calibration for one of the Mark III datasets. We have applied our likelihood analysis to the Mark III data revised accordingly, and found negligible changes in the resulting power spectrum and cosmological parameters, smaller than the uncertainties due to global zero-point discussed in § 6.2.

The close agreement between the mass power spectra derived from the two datasets indicates that the results presented here are quite robust and are unlikely to arise form specific peculiarities of either of the two samples. This does not preclude possible differences that are not picked up by the specific statistic used – in our case, the mass PS. In particular, the difference in the two bulk flows, which is known to exist, is not reflected in the power spectra. This is because the wavenumbers corresponding to the bulk velocity are smaller than the k range that dominates the fit in our current analysis.

7. CONCLUSION

We used a linear maximum-likelihood method to measure the mass-density power spectrum from the SFI catalog of peculiar velocities, and to determine the cosmological parameters for families of physical CDM models with or without COBE normalization. We have corrected for biases introduced by the non-trivial selection procedure of the SFI catalog using a new semi-analytic procedure. We have verified that the results are quite insensitive to the detailed way by which we implement this bias correction. This approach allows also to refine the distance errors estimates. Our new version of likelihood analysis enabled us to independently verify the error estimates of the SFI catalog to within an uncertainty as small as 5% of the error, which we regard as very encouraging. Since the errors affect the PS in a systematic way, this independent confirmation adds significantly to our confidence in the results.

The general result for all the models examined here is that the power spectrum at $k = 0.1\,h\,\mathrm{Mpc}^{-1}$ is $P(k)\Omega^{1.2} = (4.4 \pm 1.7) \times 10^3\,(h^{-1}\mathrm{Mpc})^3$, and that $\sigma_8\Omega^{0.6} = 0.82 \pm 0.12$. These results are obtained by the peculiar-velocity data independent of the specific shape assumed for the PS, and are consistent with the result of the Γ model independent of the COBE normalization. The random errors quoted are 90% confidence level and they include small variations due to the choice of model for the PS within the families of models tried here.

For the general family of COBE-normalized CDM models, we find a high-likelihood ridge in the $\Omega - n - h$ parameter space, which can be crudely approximated by $\Omega\, n^{\nu}\, {h_{60}}^{\mu} = 0.62 \pm 0.15$, where for ΛCDM $\mu = 1.3$ and $\nu = 2.0, 3.9$, without and with tensor fluctuation respectively. For OCDM , without tensor fluctuations, the powers are $\mu = 0.9$ and $\nu = 1.4$. Again, the error quoted is the formal 90% uncertainty including the model variations. Thus, for $h = 0.6$, the maximum-likelihood value of Ω ranges between 0.6 and unity while n varies between 1 and 0.8 respectively. Without a tilt, values of Ω as low as 0.5 are allowed within the 90% confidence limit.

Our tests using mock catalogs based on an N-body simulation that mimics our cosmological neighborhood indicate that the systematic errors in our results are relatively small. In particular, the nonlinear effects in the mock catalogs are found to be negligible. This is indeed expected because the quantity we actually measure is the velocity power spectrum in the mildly-nonlinear regime, which we have demonstrated to be reasonably approximated by linear theory. An ad-hoc test for nonlinear (multi-streaming) effects in the data themselves indicated that they may work to reduce the values of the cosmological parameters given above, but that this effect is not larger than $\sim 15\%$. In order to refine our estimates of the systematic effects even further, we intend to repeat the current analysis using a proper nonlinear scheme, and to repeat the tests of the method using simulations of higher resolution which are in preparation. We thus estimate the total systematic uncertainty to be of order $\sim 15\%$, namely comparable in size to the random errors. Therefore, to be on the safe side when comparing our results to other results, we recommend as a rule of thumb multiplying the quoted errors by a factor of ~ 2.

As yet another word of caution, it is worth recalling that our analysis is heavily weighted by the galaxies at relatively small distances, because the data is weighted by the inverse squared of the distance errors. This means that the result is sensitive to the data and error estimate of the inner galaxies. It is possible in principle that a source of distance error which operates preferentially at small distances has somehow escaped our attention and is not properly modeled by our error model. To test the effect of such a possibility, we have repeated the analysis after pruning all galaxies with distances smaller than a given distance. When pruning inside $15\,h^{-1}$Mpc (3% of the data) we obtain for the most likely value $\sigma_8\Omega^{0.6} = 0.85$ instead of the original result of $\sigma_8\Omega^{0.6} = 0.81$ when using all the data (still with our standard pruning based on linewidth). When pruning inside $25\,h^{-1}$Mpc (17% of the galaxies), we obtain instead $\sigma_8\Omega^{0.6} = 0.71$. It is encouraging to find that these variations are within the 90% likelihood contours of the different cases in the $\Omega - n$ plane, but this is yet another potential source of uncertainty to bear in mind.

A systematic trend does seem to show up when we eliminate as much as the whole inner half of the data (inside a distance of $46\,h^{-1}$Mpc, or with linewidth smaller than 2.48); the outer data, when analyzed by themselves, indicate a significantly lower PS then the inner data. This effect is not reproduced in the mock catalogs and is therefore not likely to represent a general fault in the method. Possible explanations for this effect are larger uncertainty in our estimate of random and systematic errors at large distances, differences between the assumed and the true TF relation, or a true PS with a different shape than our models. It may also be due to a real difference between the density fields in the two halves (that is somehow not properly reproduced in the simulation) or to a systematic dependence of velocity bias on galaxy properties. We carried out a number of tests in which we added to the likelihood analysis ad-hoc free parameters which allow more flexibility in the distance dependence. These include variations in the TF parameters and in the errors as a function of linewidth. Our tests indeed led to some improvement in the agreement between the two subsamples, but, being only preliminary, they did not yield so far a firm conclusion as for the dominant source of the effect and the optimal way to deal with it. Since the variations introduced preferentially affect the peculiar velocities of galaxies at large distances, which typically have large errors and therefore contribute only little to the likelihood procedure, they do not affect significantly the resultant power spectrum from the full sample. We therefore conclude that our current results are robust, and defer a more thorough investigation of this trend to a future analysis.

The recovered mass power spectrum, and the constraints on the cosmological parameters obtained here, are consistent with the results of a similar analysis applied to the Mark III catalog of peculiar velocity. This is despite the fact that these two catalogs seem to differ in some of their other properties, such as the large-scale bulk velocity. Indeed, the bulk velocity is not expected to contribute to the density on smaller scales. There is also an apparent disagreement between the results obtained from peculiar velocities of clusters (Borgani *et al.* 1997) and our result for the SFI field galaxies.

As mentioned in the Introduction, our dynamical result of $\tilde{\sigma}_8 \equiv \sigma_8 \Omega^{0.6} \simeq 0.8 \pm 0.2$ may be crudely compared to estimates of the β parameter obtained when comparing the same SFI data to a redshift survey of galaxies. da Costa *et al.* (1998) find $\beta = 0.6 \pm 0.1$ when comparing the SFI peculiar velocities to the velocities predicted by the IRAS 1.2 Jy redshift survey, assuming linear biasing. A similar value was obtained from Mark III when the comparison was done via velocities (Davis *et al.* 1996). With $\sigma_{8\mathrm{g}} \simeq 0.7$ for IRAS galaxies, the predicted β from our current constraint on $\tilde{\sigma}_8$, via $\beta = \tilde{\sigma}_8/\sigma_{8\mathrm{g}}$, is significantly closer to unity than to 0.6 (compare also to Kolatt & Dekel 1997, Fig. 6). The residuals between the measured peculiar velocities and the IRAS predictions, for the best-fit β value, were found in this comparison (da Costa *et al.* 1998) to be significantly higher than the errors as originally estimated for the SFI data (based on the scatter observed in the SCI cluster sample) combined with the errors estimated for the IRAS data.

One possibility is that the the IRAS model fails to predict some of the peculiar velocities that exist in the SFI data, e.g., because the distribution of galaxies is not properly approximated by a simple, linear, scale-independent and deterministic biasing relation (*e.g.*, Dekel & Lahav 1998). In that case, the interpretation of the value of β determined from fitting the IRAS predictions to the velocity data is not clear.

On the other hand, it is also possible that the errors in SFI are indeed larger than originally estimated. Such larger errors would accordingly reduce the PS amplitude, in particular the value of $\tilde{\sigma}_8$, as estimated in the current paper. However, such an effect should have been detected by investigating the global biasing properties of the sample. It would also be hard to understand why our likelihood analysis does prefer errors very similar to the original estimates. Although we are fairly convinced that nonlinear effects in the current analysis are confined to the level of $\leq 15\%$, it will be worth making an extra effort to improve the accuracy in a future paper.

We thank George Blumenthal, Stefano Borgani, Gerard Lemson, Adi Nusser, and Michael Strauss for stimulating discussions. We are grateful to the ESO Visitors fund for supporting visits to Garching by AD, GW, IZ, MPH, and RG. This research was supported in part by an ESO DGDF grant to WF, the US-Israel Binational Science Foundation grant

95-00330 and the Israel Science Foundation grant 950/95 to AD, IZ and AE, the DOE and the NASA grant NAG 5-7092 at Fermilab to IZ, NSF grants AST94-20505 and AST96-17069 to RG, AST95-28860 to MPH, and AST93-47714 to GW.

REFERENCES

Bardeen, J. M., Bond, J. R., Kaiser, N., & Szalay, A. S. 1986, ApJ, 304, 15

Bennett, C. L., *et al.* 1996, ApJ, 464, L1

Bothun, G. D., Mould, J. R. 1987, ApJ, 313, 629

Borgani, S., da Costa, L. N., Freudling, W., Giovanelli, R., Haynes, M. P., Salzer, J. & Wegner, G., 1997, ApJ, 482, L121

Colberg, J. M. *et al.* 1999, in preparation

da Costa, L. N., Freudling, W., Wegner, G., Giovanelli, R., Haynes, M. P., & Salzer, J. J. 1996, ApJ, 468, L5

da Costa, L. N., Nusser, A., Freudling, W., Giovanelli, R., Haynes, M. P., Salzer, J. J., & Wegner, G. 1998, MNRAS, 299, 425

Davis, M., Nusser, A., & Willick, J. A. 1996, ApJ, 473, 22

Dekel, A. 1998, in *Formation of Structure in the Universe*, eds. A. Dekel & J. P. Ostriker, Cambridge: Cambridge University Press, 250

Dekel, A., Bertchinger, E., & Faber, S. M. 1990, ApJ, 364, 349

Dekel, A., Eldar, A., Kolatt, T., Yahil, A., Willick, J. A., Faber, S. M., Courteau, S., & Burstein, D. 1998, ApJ, submitted (astro-ph/9812197)

Dekel, A., & Lahav, O. 1998, ApJ, submitted (astro-ph/9806193)

Efstathiou, G., Bond, J. R., & White, S. D. M. 1992, MNRAS, 258, 1p

Eldar, A. *et al.* 1999, in preparation

Fisher, K. B., Huchra, J. P., Strauss, M. A., Davis, M., Yahil, A., & Schlegel, D. 1995, ApJS, 100, 69

Freudling, W., da Costa, L. N., Pellegrini, P. S. 1994, MNRAS, 268, 943

Freudling, W., da Costa, L. N., Wegner, G., Giovanelli, R., Haynes, M. P., & Salzer, J. J. 1995, AJ, 110, 920

Freudling, W., Martel, H., Haynes, M. P. 1991, ApJ, 377, 349

Giovanelli, R., Haynes, M. P., Herter, T., Vogt, N., Salzer, J. J., Wegner, G., da Costa, L. N., & Freudling, W. 1997a, AJ, 113, 22

Giovanelli, R., Haynes, M. P., Herter, T., Vogt, N., da Costa, L. N., & Freudling, W., Salzer, J. J., Wegner, G. 1997b, AJ, 113, 53

Giovanelli, R., Haynes, M. P., Freudling, W., Da Costa, L. N., Salzer, J. J., & Wegner, G. 1998a, ApJ, 505, L91

Giovanelli, R., Haynes, M. P., Salzer, J. J., Wegner, G., Da Costa, L. N., & Freudling, W. 1998b, AJ, 116, 2632

Górski, K. M. 1988, ApJ, 332, L7

Górski, K. M., Davis, M., Strauss, M. A., White, S. D. M., & Yahil, A. 1989, ApJ, 344, 1

Górski, K. M., Ratra, B., Stompor, R., Sugiyama, N., & Banday, A. J. 1998, ApJS, 114, 1

Górski, K. M., Ratra, B., Sugiyama, N., & Banday, A. J. 1995, ApJ, 444, L65

Groth, E. J., Juszkiewicz, R., & Ostriker, J. P. 1989, ApJ, 346, 558

Hinshaw, G., Banday, A. J., Bennett, C. L., Gorski, K. M., Kogut, A., Smoot, G. F., & Wright, E. L. 1996, ApJ, 464, L17

Haynes, M. P. *et al.* 1999, in preparation

Jaffe, A. H., & Kaiser, N. 1995, ApJ, 455, 26

Jain, B., Mo., H. J., & White, S. D. M. 1995, MNRAS, 276, L25

Kashlinsky, A. 1998, ApJ, 492, 1

Kaiser, N. 1988, MNRAS, 231, 149

Kofman, L., Bertschinger, E., Gelb, J. M., Nusser, A., & Dekel, A. 1994, ApJ, 420, 44

Kolatt, T., & Dekel, A. 1997, ApJ, 479, 592

Kolatt, T., Dekel, A., Ganon, G., & Willick, J. A. 1996, ApJ, 458, 419

Mathewson, D. S., Ford, V. L., & Buchhorn, M. 1992, ApJS, 81, 413

Peacock, J. A., & Dodds, S. J. 1994, MNRAS, 267, 1020

Peacock, J. A., & Dodds, S. J. 1996, MNRAS, 280, L19

Sigad,Y., Dekel, A., Eldar, A., Strauss, M., Yahil, A. 1998, ApJ, 495, 516

Strauss, M. A. 1998, in *Formation of Structure in the Universe*, eds. A. Dekel & J. P. Ostriker, Cambridge: Cambridge University Press, 172

Strauss, M. A., & Willick, J. A. 1995, Phys. Rep., 261, 271

Sugiyama, N. 1995, ApJS, 100, 281

Tytler, D, Fan, X-M, & Burles, S. 1996, Nature, 381, 207

Wegner, M. P. *et al.* 1999, in preparation

White, M., & Bunn, E. F. 1995, ApJ, 450, 477

Willick, J. A., Courteau, S., Faber, S. M., Burstein, D., & Dekel, A. 1995, ApJ, 446, 12

Willick, J. A., Courteau, S., Faber, S. M., Burstein, D., Dekel, A., & Kolatt, T. 1996, ApJ, 457, 460

Willick, J. A., Courteau, S., Faber, S. M., Burstein, D., Dekel, A., & Strauss, M. A. 1997a, ApJS, 109, 333

Willick, J. A., & Strauss, M. A. 1998, ApJ, 507, 64

Willick, J. A., Strauss, M. A., Dekel, A., & Kolatt, T. 1997b, ApJ, 486, 629

Zaroubi, S., Zehavi, I., Dekel, A., Hoffman, Y., & Kolatt, T. 1997, ApJ, 486, 21

Zehavi, I. *et al.* 1999, in preparation